Small world of Ulam networks for chaotic Hamiltonian dynamics

Klaus M. Frahm and Dima L. Shepelyansky

Laboratoire de Physique Théorique, IRSAMC, Université de Toulouse, CNRS, UPS, 31062 Toulouse, France

We show that the Ulam method applied to dynamical symplectic maps generates Ulam networks which belong to the class of small-world networks appearing for social networks of people, actors, power grids, biological networks, and Facebook. We analyze the small-world properties of Ulam networks on examples of the Chirikov standard map and the Arnold cat map showing that the number of degrees of separation, or the Erdös number, grows logarithmically with the network size for the regime of strong chaos. This growth is related to the Lyapunov instability of chaotic dynamics. The presence of stability islands leads to an algebraic growth of the Erdös number with the network size. We also compare the time scales related with the Erdös number and the relaxation times of the Perron-Frobenius operator showing that they have a different behavior.

I. INTRODUCTION

In 1960 Ulam proposed a method [1], known now as the *Ulam method*, for generating discrete, a finite cell approximate of the Perron-Frobenius operator for a chaotic map in a continuous phase space. The transition probabilities from one cell to the others are determined from an ensemble of trajectories which generates the probabilities of Markov transitions [2] between cells after one map iteration. In this way the Ulam method produces the Ulam networks with weighted probability transitions between nodes corresponding to phase-space cells. For one-dimensional (1D) fully chaotic maps [3,4] the convergence of the discrete dynamics of this Ulam approximate of the Perron-Frobenius operator (UPFO), at cell size going to zero to the continuous dynamics has been mathematically proven in Ref. [5]. The properties of UPFO was studied for 1D [6–8] and 2D [9–12] maps. It was shown that the UPFO finds useful applications for analysis of dynamics of molecular systems [13] and coherent structures in dynamical flows [14]. Recent studies [15,16] demonstrated similarities between the UPFO, corresponding to Ulam networks, and the Google matrix of complex directed networks of World Wide Web, Wikipedia, world trade, and other systems [17–19].

From a physical point of view the finite cell size of UPFO corresponds to the introduction of a finite noise with amplitude given by a discretization cell size. For dynamical maps with a divided phase space, like the Chirikov standard map [20], such a noise leads to the destruction of invariant Kolmogorov-Arnold-Moser (KAM) curves [3,20,21] so that the original Ulam method is not operating in a correct way for such maps. However, the method can be considered in its generalized form [22] when the Markov transitions are generated by specific trajectories starting only inside one chaotic component thus producing Markov transitions between cells belonging only to this chaotic component. Due to ergodicity on the chaotic component even only one long chaotic trajectory can generate a complete UPFO avoiding the destruction of KAM curves and stability islands. It was also shown numerically that the spectrum of the finite-size UPFO

matrix converges to a limiting density at cell sizes going to zero [22].

Certain similarities between the spectrum of UPFO matrices of Ulam networks and those of a Google matrix of complex directed networks have already been discussed in the literature (see, e.g., Ref. [19]). Here we address another feature of Ulam networks showing that they have small-world properties, meaning that almost any two nodes are indirectly connected by a small number of links. Such a small-world property with its *six degrees of separation* is typical for social networks of people [23], actors, power grids, and biological and other networks [24–26]. Thus the whole Facebook network of about 700 million users has only four degrees of separation [27].

The paper is organized as follows: Section II presents the main properties of the two symplectic maps considered; construction of Ulam networks is described in Sec. III; small-world properties of Ulam networks are analyzed in Sec. IV; and the relaxation rates of the coarse-grained Perron-Frobenius operator are considered in Sec. V. The obtained results are discussed in the Sec. VI.

II. DYNAMICAL SYMPLECTIC MAPS

We analyze the properties of Ulam networks for two examples, the Chirikov standard map [20] and the Arnold cat map [21]. Both maps capture the important generic features of Hamiltonian dynamics and find a variety of applications for the description of real physical systems (see, e.g., Ref. [28]).

The Chirikov standard map has the form:

$$\bar{p} = p + \frac{K}{2\pi}\sin(2\pi x) , \quad \bar{x} = x + \bar{p} \pmod 1. \quad (1)$$

Here bars mark the variables after one map iteration and we consider the dynamics to be periodic on a torus so that $0 \leqslant x \leqslant 1$, $0 \leqslant p \leqslant 1$. It is argued that the last KAM curve is the one with the golden rotation number being destroyed at critical $K_c = K_g = 0.971635406\ldots$ [29]. Indeed, further mathematical analysis [30] showed that all KAM curves are

destroyed for $K \geqslant 63/64$ while the numerical analysis [31] showed that $K_c - K_g < 2.5 \times 10^4$. Thus it is most probable that $K_c = K_g$ and the golden KAM curve is the last to be destroyed (see also the review in Ref. [32]).

The Arnold cat map [21] of the form

$$\bar{p} = p + x \pmod{L}, \quad \bar{x} = x + \bar{p} \pmod{1}, \qquad (2)$$

is the cornerstone model of classical dynamical chaos [3]. This symplectic map belongs to the class of Anosov systems; it has the positive Kolmogorov-Sinai entropy $h = \ln[(3 + \sqrt{5})/2)] \approx 0.9624$ and is fully chaotic [3]. Here the first equation can be seen as a kick which changes the momentum p of a particle on a torus while the second one corresponds to a free phase rotation in the interval $-0.5 \leqslant x < 0.5$; bars mark the new values of canonical variables (x, p). The map dynamics takes place on a torus of integer length L in the p direction with $-L/2 < p \leqslant L/2$. The usual case of the Arnold cat map corresponds to $L = 1$ but it is more interesting to study the map on a torus of longer integer size $L > 1$ generating a diffusive dynamics in p [33,34]. For $L \gg 1$ the diffusive process for the probability density $w(p, t)$ is described by the Fokker-Planck equation:

$$\frac{\partial w(p, t)}{\partial t} = \frac{D}{2} \frac{\partial^2 w(p, t)}{\partial p^2}, \qquad (3)$$

with the diffusion coefficient $D \approx \langle x^2 \rangle = 1/12$ and t being iteration time. As a result, for times $t \gg L^2/D$ the distribution converges to the ergodic equilibrium with a homogeneous density in the plane (x, p) [34].

III. CONSTRUCTION OF ULAM NETWORKS

We construct the Ulam network and related UPFO for the map (1) as described in Ref. [22]. First we reduce the phase space to the region $0 \leqslant x < 1$ and $0 \leqslant p < 0.5$ exploiting the symmetry $x \to 1 - x$ and $p \to 1 - p$. The reduced phase space is divided into $M \times (M/2)$ cells with certain integer values M in the range $25 \leqslant M \leqslant 3200$. To determine the classical transition probabilities between cells we iterate one very long trajectory of 10^{12} iterations starting inside the chaotic component at $x = p = 0.1/(2\pi)$ and count the number of transitions from a cell i to a cell j. Depending on the value of K it is possible that there are stable islands or other nonaccessible regions where the trajectory never enters. This corresponds to certain cells that do not contribute to the Ulam network. In practice, we perform trajectory iterations only for the largest two values $M = 3200$ and $M = 2240$ and apply an exact renormalization scheme to reduce successively the value of M by a factor of 2 down to $M = 25$ and $M = 35$ (for these two cases the vertical cell number is chosen as $(M + 1)/2$ with the top line of cells only covering half cells). We consider the dynamics for four different values of K: the golden critical value $K = K_g = 0.971635406$, $K = 5$, $K = 7$, and $K = 7 + 2\pi$. There are small stability islands for the last three cases. The original Ulam method [1] computes the transition probabilities from one cell to other cells using many random initial conditions per cell but for the Chirikov standard map this would imply that the implicit coarse graining of the method produces a diffusion into the stable islands or other classically nonaccessible regions which we want to

avoid. The typical network size (of contributing nodes/cells) is approximately $N_d \approx M^2/2$ ($N_d \approx M^2/4$) for the cases with $K \geqslant 5$ ($K = K_g$).

For the Arnold cat map (2) we divide the phase space $-0.5 \leqslant x < 0.5$ and $-L/2 \leqslant p < L/2$ into $M \times LM$ cells where in this work we mostly choose $L = 3$ and M is taken from a sequence of prime numbers starting with $M = 29$ and increasing M roughly by a factor of 1.4 in order to minimize certain arithmetic effects from nonprime numbers. Since the Arnold cat map does not have any inaccessible regions, both variants of the Ulam method, with many random initial conditions or one long trajectory (using a suitable irrational choice of the initial position), work very well.

However, due to the exact linear form of (2) it is even possible to compute directly very *efficiently* and *exactly* (without any averaging procedure) the transition probabilities. Details of this procedure for the Arnold cat map together with a discussion of related properties of the UPFO for the standard map are given in Appendix. The results for the UPFO for the cat map given below in this work have all been obtained for the exact UPFO computed in this way.

IV. SMALL-WORLD PROPERTIES OF ULAM NETWORKS

To study the small-world properties of the Ulam networks we compute a quantity which we call the Erdös number N_E (or number of degrees of separation) [26,35]. This number represents the minimal number of links necessary to reach indirectly a specific node via other intermediate nodes from a particular node called the hub. Here the (nonvanishing) transition probabilities are not important and only the existence of a link between two nodes is relevant. The recursive computation of N_E for all nodes can be done very efficiently for large networks by keeping a list of nodes with same N_E found in the last iteration and which is used to construct a new list of nodes with N_E increased by unity as all nodes being connected to a node of the initial list and not yet having a valid smaller value of N_E (for nodes found in a former iteration). After each iteration the list will be updated with the new list and the initial list of this procedure at $N_E = 0$ is chosen to contain one node being the hub.

Figure 1 shows the probability distributions $w_E(N_E)$ of the Erdös number N_E [using a hub cell at $x = 0.1/(2\pi)$, $p = 0$] and the number of links N_l per node of the UPFO for the Chirikov standard map at $K = 7$ and $K = 7 + 2\pi$ for the three largest values of $M = 1600, 2240, 3200$ considered. The distributions of N_E are quite sharp with mean values of N_E around 8 (or 7) for $K = 7$ ($K = 7 + 2\pi$) being slightly increasing with M. Even though the maximal possible values are larger [$N_E^{(\max)} = 33$ for $K = 7$ and $N_E^{(\max)} = 21$ for $K = 7 + 2\pi$ at $M = 3200$] the big majority of nodes have a value $N_E \leqslant 12$ (10) for $K = 7$ ($K = 7 + 2\pi$), clearly confirming the small-world structure of these networks.

The corresponding distribution $w_l(N_l)$ of number of links N_l shows that N_l takes essentially only even values in the range $4 \leqslant N_l \leqslant N_l^{(\max)}$ with $N_l^{(\max)} = 18$ (32) for $K = 7$ ($K = 7 + 2\pi$). This behavior can be understood in the framework of the discussion in Appendix showing that the image of an initial square cell is (up to nonlinear corrections) a parallelogram with extreme points (relative to a certain reference
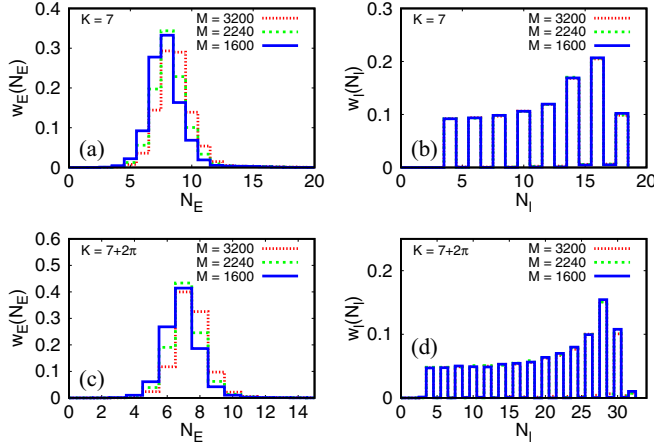
FIG. 1. Left panels: Probability distribution w_E of Erdös number N_E for the Ulam network of the Chirikov standard map at $K = 7$ (a) and $K = 7 + 2\pi$ (c) for three different numbers of nodes (cells) $N_d \approx M^2/2$ using a hub cell at $x = 0.1/(2\pi)$, $p = 0$. [(b) and (d)] Probability distribution w_l of number of links N_l per node of the networks of panels (a) and (c), respectively. In all cases the Ulam network was constructed with one trajectory of 10^{12} iterations using the initial condition $x = 0.1/(2\pi)$, $p = 0.1/(2\pi)$.

cell) $\Delta s(\xi_0, \xi_0)$ and $\Delta s(\xi_0 + A + 2, \xi_0 + A + 1)$, where ξ_0 is a quasirandom uniformly distributed quantity in the interval $\xi_0 \in [0, 1[$ and $\Delta s = 1/M$ is the linear cell size. Here we assume that $A = K \cos(2\pi \Delta s \, x_i) > 0$ (the argumentation for $A < 0$ is rather similar with $A \to |A|$). The parallelogram covers in horizontal direction nearly always two cells and in diagonal direction $\lceil \xi_0 + A + 1 \rceil \geqslant 2$ cells where $\lceil u \rceil$ is the ceil function of u being the smallest integer larger or equal than u. Therefore typical values of $N_l = 2\lceil \xi_0 + A + 1 \rceil$ are indeed even numbers with $4 \leqslant N_l \leqslant N_l^{(\text{max})}$, where $N_l^{(\text{max})} = 2\lceil 2 + K \rceil$ is in agreement with the observed values in Fig. 1.

Actually for $K = 7 + 2\pi \approx 13.283$ we also understand that the probability for $N_l = N_l^{(\text{max})} = 32$ is quite strongly reduced because even for maximal $A = K$ we need that the offset satisfies $\xi_0 > 1 - 0.283$ which is statistically less likely. Apart from this there is also a slight increase of histogram bins with larger values of N_l due to the cosine factor in A applied on a uniformly distributed phase. For sufficiently large M this argumentation does not depend on system or network size. We mention that for very small values of M there are deviations from this general picture, with some small probabilities for odd values of N_l due to boundary effects, also related to stable islands and inaccessible phase-space regions (especially for $K = K_g$). For the largest values $M = 3200$, 2240 and $K = 7 + 2\pi$ the figure shows some small deviations due to statistical fluctuations since the average ratio of trajectory transitions per link $10^{12}/[N_d N_l^{(\text{max})}] \approx 6000$ is rather modest. Furthermore, the data for $K = 5$ (not shown in Fig. 1) are also in agreement with this general picture with $N_l^{(\text{max})} = 14$ and typically $N_E \approx 11 \pm 3$.

According to Fig. 2 the average Erdös number for the three cases with $K \geqslant 5$ behaves approximately as

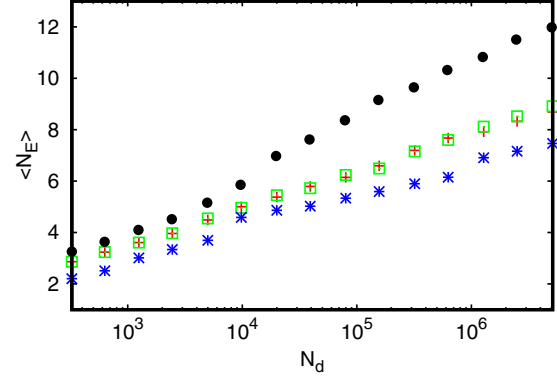$$\langle N_E \rangle \approx C_1 + C_2 \ln(N_d). \tag{4}$$

FIG. 2. Dependence of the average Erdös number $\langle N_E \rangle$ on the number of nodes (cells) N_d for the Ulam network of the Chirikov standard map at $K = 5$ (top data points, black dots), $K = 7$ (both sets of center data symbols of red pluses and green squares), and $K = 7 + 2\pi \approx 13.28$ (bottom data points, blue stars). The hub cell is either at $x = 0.1/(2\pi)$, $p = 0$ (top, center with red plus symbols and bottom) or at $x = 0.1/(2\pi)$, $p = 0.1/(2\pi)$ (center data with green squares).

Here C_1, C_2 are some numerical constants which have no significant dependence on the hub choice as long it is not close to some stable island or similar. The typical values of C_2 are close to h^{-1} with $h = \ln(K/2)$ being the Lyapunov exponent of the standard map (for $K > 4$) [20]. This is due to the theoretically expected behavior $N_f(N_E) \approx e^{hN_E}$ for $N_E < \langle N_E \rangle$ and where $N_f(N_E) = N_d w_E(N_E)$ is the number of cells indirectly connected to the hub after N_E iterations. This theoretical behavior is rather well confirmed by the data of the left panel of Fig. 1 (when presented in log presentation for the y axis and multiplied with N_d). The exponential increase saturates at $N_E = \langle N_E \rangle$ with $e^{h\langle N_E \rangle} \approx \alpha N_d$ and α being a constant of order of unity implying $C_2 = 1/h$ and $C_1 = \ln(\alpha)/h$.

We have performed a similar analysis of N_l and N_E also for the Arnold cat map. Here the link number N_l is constant for all nodes with values 4, 5, or 6 depending on the parity of M or LM as explained in Appendix. The behavior of N_E is presented in Fig. 3 showing the frequency distribution $N_f(N_E) = N_d w_E(N_E)$ (left panel) and the dependence $\langle N_E \rangle$ on N_d (right panel) for $L = 3$ and several (prime) values of M. The expected theoretical behavior of both quantities is very clearly confirmed providing accurate fit values of the Lyapunov exponent being numerically very close to the theoretical value $h_{\text{th}} = \ln[(3 + \sqrt{5})/2] \approx 0.9624$. Furthermore, the saturation of the exponential growth of $N_f(N_E)$ for $N_E \geqslant \langle N_E \rangle$ happens quite abruptly with $N_E^{(\text{max})} = \langle N_E \rangle + 3$. We also computed the restricted average of N_E over the center square box (of $L = 3$ squares) with $|x| < 0.5$ and $|p| < 0.5$ which turns out to be quite close to the full average with $|x| < 0.5$ and $|p| < L/2$ showing that for the Erdös number the diffusive dynamics is apparently not very relevant.

To understand the spatial structure of the Erdös number of nodes we show in top panels of Fig. 4 density plots of the phase-space probability distribution after a few iterations of the UPFO for the map (1) at $K = 7$ and $M = 400$ applied to an initial cell state. One can clearly identify the chaotic
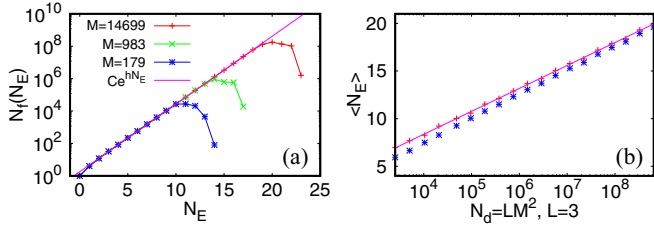
FIG. 3. Properties of the Erdös number N_E for the Ulam network of the Arnold cat map on a torus with $L = 3$ with hub cell at position $x = p = 0$. (a) Frequency distribution $N_f(N_E)$ for three different values of M. The pink line corresponds to the fit $N_f(E) = C e^{hN_E}$ for $M = 14\,699$ using the fit range $2 \leqslant N_E \leqslant 18$ with $C = 1.777 \pm 0.005$ and $h = 0.9629 \pm 0.0002$. (b) Dependence of average $\langle N_E \rangle$ on the number of nodes (cells) $N_d = LM^2$ (red plus symbols). The blue stars correspond to a restricted average over nodes being in the center square box with $|x| < 0.5$ and $|p| < 0.5$ (instead of $|x| < 0.5$ and $|p| < L/2$ for the full average). The pink line corresponds to the fit (of top data points) $\langle N_E \rangle = d + \ln(N_d)/\tilde{h}$ with $d = -1.25 \pm 0.08$ and $\tilde{h} = 0.957 \pm 0.005$. The two values of h and $\tilde{h}$ compare to the theoretical Lyapunov exponent $h_{\text{th}} = \ln[(3 + \sqrt{5})/2] \approx 0.9624$. The Ulam network for the Arnold cat map was constructed from exact theoretical transition probabilities as described in Appendix. The number of links per node is constant for all nodes: $N_l = 5$ (4 or 6) if M and LM are odd (M and LM even or M odd and LM even, respectively).

spreading along a one-dimensional manifold which fills up the phase space due to refolding induced by the periodic boundary conditions. The lower panels show the full spatial distribution of the Erdös number by a color plot using red (green, light blue) for nodes with smallest (medium, largest) Erdös number. Dark blue is used for nonaccessible nodes in the stable islands which have no Erdös number. Furthermore, for a better visibility we consider a full square box with $0 \leqslant x < 1$ and $-0.5 \leqslant p < 0.5$, where the data for $p < 0$ is obtained by the transformation $x \to 1 - x$ and $p \to -p$ from the data with $p \geqslant 0$. In this way the two small stable islands at $p = 0$ for $K = 7$ have a full visibility (the influence of orbits sticking near these islands on Poincaré recurrences is discussed in Ref. [36]). Nodes with the smallest Erdös number follow the same one-dimensional unstable manifold as the chaotic stretching and nodes with maximal Erdös number are close to the outer boundaries of the stable islands which are last reached when starting from the hub.

Figure 5 shows the probability distributions of N_E and N_l for the standard map at the golden critical value $K = K_g = 0.971635406$ with a complicated structure of stable islands inside the main chaotic component. The distribution of N_E is now rather large with nonvanishing probabilities at values $N_E \sim 10^2$ and several local maxima due to the complicated phase-space structure with different layers of initial diffusive spreading (limited by the golden curve). The distribution of N_l is mostly concentrated on the two values $N_l = 4$ and 6 in agreement with the above discussion since $N_l^{(\text{max})} = 2\lceil 2 + K_g \rceil = 6$.

The spatial distribution of N_E for $K = K_g$ [using a hub cell at $x = 0.1/(2\pi)$ and $p = 0$] is illustrated in the top panel of Fig. 6 by the same type of color plot used for the lower
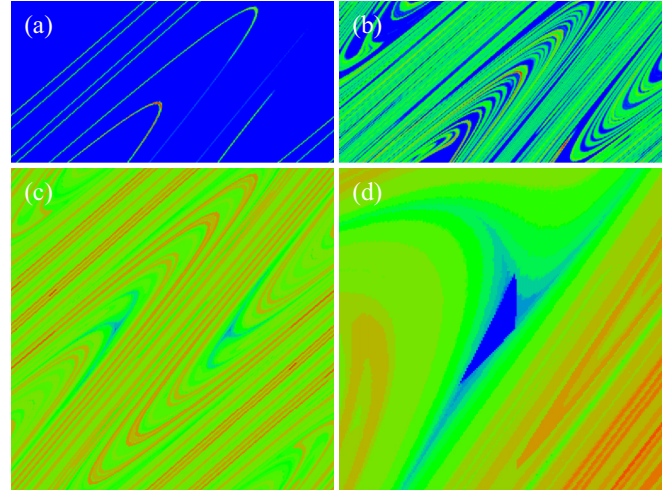

FIG. 4. Top: Color density plot of the probability distribution in the phase plane (x, p) obtained after $t = 4$ (a) or $t = 7$ (b) iterations of the UPFO ($M = 400$, resolution 400×200 boxes) for the Chirikov standard map at $K = 7$ with an initial state being localized in one cell at $x = p = 0.1/(2\pi)$. The colors red, green, and blue correspond to maximum, medium, and minimal values. (c) Density plots of the Erdös number of nodes or cells for the Ulam network (standard map, $K = 7$, same hub position as in Fig. 1) in the phase plane (x, p) with red, green, and light blue corresponding to smallest, medium, and largest Erdös numbers. The dark blue cells correspond to nonaccessible islands which do not contribute as nodes for the Ulam network. Left panel corresponds to one full square box of the phase space given by $0 \leqslant x < 1$ and $-0.5 \leqslant p < 0.5$ for $M = 400$ (resolution 400×400 boxes). Panel (d) shows a zoom of 200×200 cells with bottom left corner at cell position (935,1500) for $M = 3200$ and containing the left of the two islands (for $K = 7$). In both bottom panels data for cells with $p < 0$ are obtained from the symmetry: $p \to -p$ and $x \to 1 - x$.

panels of Fig. 5. In this case N_E follows clearly the (very slow) diffusive spreading with smallest N_E values in the layers close to the hub and maximal N_E values closest to the top layers just below the golden curve.

The bottom panel of Fig. 6 shows the N_E color plot (with hub cell at $p = x = 0$) for the Arnold cat map at $L = 3$ and the rather small value $M = 59$ for a better visibility. As for the case $K = 7$ of map (1) the Erdös number follows a one-dimensional unstable manifold (a straight refolded line for the cat map) and the chaotic spreading reaches quite quickly the two outer square boxes (with $|p| > 0.5$). We have verified that this behavior is also confirmed by the corresponding N_E
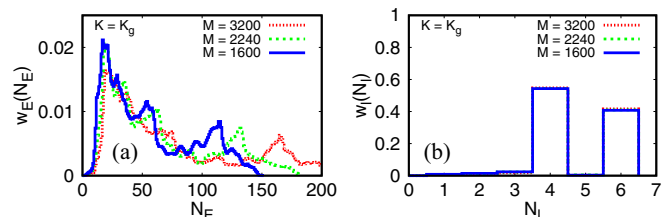

FIG. 5. Same as in Fig. 1 but for the golden critical value $K = K_g = 0.971635406$ of map (1).
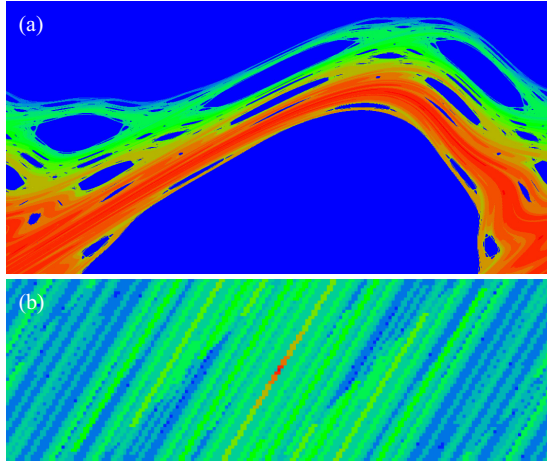
FIG. 6. Density plots of Erdös number (similar as in bottom panels of Fig. 4) for the Ulam network of the Chirikov standard map at the golden critical value $K = K_g = 0.971635406$ for $M = 3200$ [top panel (a), hub cell at position $x = 0.1/(2\pi)$, $p = 0$, resolution 3200×1600 boxes] and of the Arnold cat map for $M = 59$, $L = 3$ [bottom panel (b), hub cell at position $x = p = 0$, resolution 59×177 boxes]. In the latter case the roles of the x and p axes have been exchanged for a better visibility.

color plots at larger values of M. The evolution of the nodes with smallest N_E values does not follow the classical diffusion which can be understood by the fact that the Erdös number only cares about reaching a cell as such even with a very small probability while the diffusive dynamics applies to the evolution of the probability occupation of each cell. This is similar to a one-dimensional random walk with a diffusive spreading $\sim \sqrt{Dt}$ of the spatial probability distribution while the Erdös number (i.e., set of "touched" cells) increases ballistically in time $\sim t$.

Figure 7 shows the dependence of the average $\langle N_E \rangle$ on N_d for $K = K_g$ which follows a power law $\langle N_E \rangle \sim N_d^b$ with $b = 0.297 \pm 0.004$. For this case the logarithmic behavior
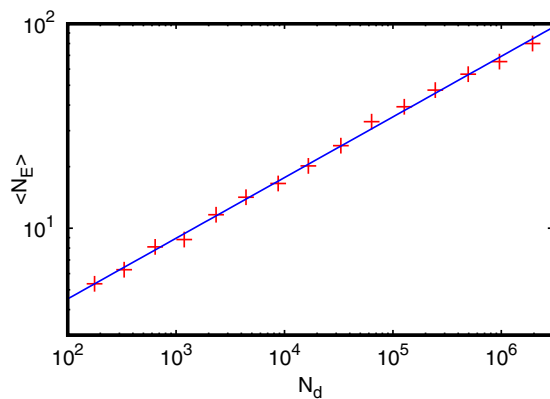

FIG. 7. Dependence of the average Erdös number $\langle N_E \rangle$ on the number of nodes (cells) N_d for the Ulam network of the Chirikov standard map at $K = K_g$ (red plus symbols) with hub cell at $x = 0.1/(2\pi)$, $p = 0$ in a double logarithmic representation. The blue line corresponds to the fit $\langle N_E \rangle = C N_d^b$ with $C = 1.15 \pm 0.04$ and $b = 0.297 \pm 0.004$.

$\langle N_E \rangle \sim \ln N_d$ (4) observed for $K \geqslant 5$ is not valid due to the small Lyapunov exponent and complicated phase-space structure with slow diffusive spreading and complications from orbits trapped around stable islands.

To explain the obtained dependence $N_E \sim N_d^{0.3}$ we give the following heuristic argument. According to the renormalization description of the critical golden curve the typical time scale of motion in the vicinity of a certain resonance with the Fibonacci approximate of the golden rotation number $r_n = q_{n-1}/q_n \to r_g = (\sqrt{5} - 1)/2$ with $q_n = 1, 2, 3, 5, 8, \ldots$ is $t_n \sim q_n$ (same for the symmetric golden curve with $r = 1 - r_g$) [29,37]. At the same time the area of one cell close to the resonance q_n with typical size $1/q_n^2$ scales approximately as $A_n \sim 1/(q_n^2 t_n) \sim 1/q_n^3$. Since a cell of the Ulam network has an area $1/N_d \sim A_n$ we obtain that $t_n \sim N_d^{1/3}$. We expect that the typical time to reach the resonance with largest q_n value that can be resolved by the UPFO discretization is of the order of the most probable Erdös number such that $N_E \sim t_n \sim N_d^{1/3}$ leading to $b = 1/3$ comparable with the obtained numerical value. Of course, this handwaving argument is very simplified since in addition to Fibonacci resonance approximates there are other resonances which play a role in long time sticking of trajectories and algebraic decay of Poincaré recurrences (see, e.g., Refs. [38–40]). Also as discussed above the Erdös number is for a network with equal weights of transitions while in the UPFO for the Chirikov standard map the transition weights are different.

Indeed, since the Erdös number does not depend on the weight w_l of a link it follows in principle a different dynamics than the UPFO applied on an initial localized state. Therefore we also analyzed the statistical distribution of link weights w_l. Figure 8 shows the integrated weight distribution $P_w(w_l)$ (fraction of links with weight below w_l) of the UPFO for the Chirikov standard map for different values of K and M. The vertical lines at some minimal value correspond to the smallest possible weight values $w_l^{(\min)} = N_d/10^{12}$ being the typical inverse number of trajectory crossings per cell and are due to the finite length of the the iteration trajectory. Apart from this, in the regime $w_l^{(\min)} < w_l < 0.1$, the behavior is very close to a power law $P_w(w_l) \sim w_l^b$ with some exponent rather close to $b \approx 0.5$ depending on K values and fit ranges. This leads to a square root singularity in the probability distribution $p_w(w_l) = P_w'(w_l) \sim w_l^{-0.5}$.

To understand this dependence we note that according to the discussion in Appendix the weights w_l are given as the relative intersection areas of a certain parallelogram (the image of one Ulam cell by the map) with the target Ulam cells and that the bottom corner point of the parallelogram (relative to its target cell) is given by $\Delta s(\xi_0, \xi_0)$, where $\xi_0 \in [0, 1[$ has a uniform quasirandom distribution (see also the bottom right panel of Fig. 11 in Appendix). If $1 - \xi_0 \ll 1$, then this provides the triangle area (relative to the cell size Δs^2) as $w_l = C(A)(1 - \xi_0)^2/2$ with a coefficient dependent on the parameter $A = K \cos(2\pi \Delta s \, x_i)$, and also if we consider the triangle in the cell around the lowest corner point or the cell right next to it (which may have a smaller area depending on A). Since ξ_0 is uniformly distributed we find (after an additional average over the initial cells, i.e., over the parameter A) immediately that $p_w(w_l) \sim w_l^{-1/2}$. It is also possible that the
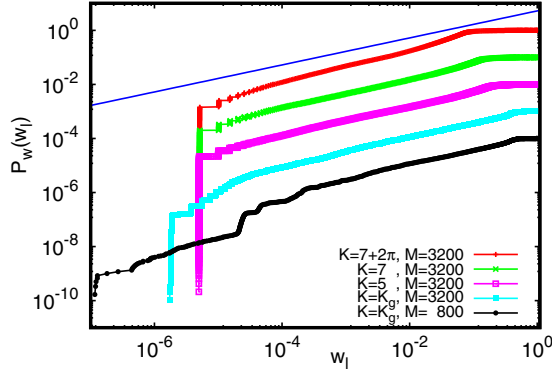
FIG. 8. Double logarithmic representation of fraction $P(w_l)$ of links with weight below w_l of the Ulam network for the Chirikov standard map with various values of K and M. The lower curves are successively shifted down by a factor of 10 for a better visibility. The top straight blue line corresponds to the simplified power law behavior $\sim w_l^{0.5}$. The power law fits $P_w(w_l) = C\, w_l^b$ for the range $5 \times 10^{-5} < w_l < 2.5 \times 10^{-2}$ for $K \geqslant 5$ ($10^{-4} < w_l < 5 \times 10^{-1}$ for $K = K_g$) provide the fit values (top to bottom curves): $C = 2.63 \pm 0.03$, 1.64 ± 0.01, 1.68 ± 0.02, 1.31 ± 0.01, 1.39 ± 0.02 and $b = 0.584 \pm 0.002$, 0.521 ± 0.001, 0.525 ± 0.002, 0.542 ± 0.001, 0.571 ± 0.003. The vertical lines of data at the left side correspond to the smallest possible weight values $N_d/10^{12}$ being the typical inverse number of trajectory crossings per cell with $N_d \approx M^2/2$ for $K \geqslant 5$ or $N_d \approx M^2/4$ for $K = K_g$.

top corner point of the parallelogram (instead of the bottom corner point) may produce the minimal weight (among all target cells for a given initial cell). However, the top corner point also lies on the diagonal (relative to its target cell) and produces therefore the same square root singularity.

The appearance of the singularity is certainly very interesting. However, this singularity is integrable and the main part of links still have weights w_l comparable to its typical value $w_l \sim N_l^{-1}$ given by the relative intersection areas of the parallelogram with the other target cells. Furthermore, despite this singularity, it seems that the dynamics of the Erdös number follows qualitatively quite well the chaotic dynamics induced by the direct application of the UPFO as can be seen, for example, in Figs. 4 and 6.

The results of this section show that in the regime of strong chaos the Ulam networks are characterized by small values of the Erdös number $N_E \sim \ln N_d$ growing only logarithmically with the network size N_d. However, the presence of stability islands can modify the asymptotic behavior leading to a more rapid growth with $N_E \sim N_d^{0.3}$ as it is the case for the critical golden curve of the Chirikov standard map where a half of the total measure is occupied by stability islands.

V. SMALL RELAXATION RATES OF UPFO

The average (or maximal) Erdös number gives the time scale at which the UPFO touches most (or all) Ulam cells when applied to an initial state localized at one cell (hub) but it does not take into account the probability density associated to the target cells which may be very small for the cells with largest N_E at iteration times $t \sim N_E^{(\text{max})}$. However, the direct iterated application of the UPFO on a
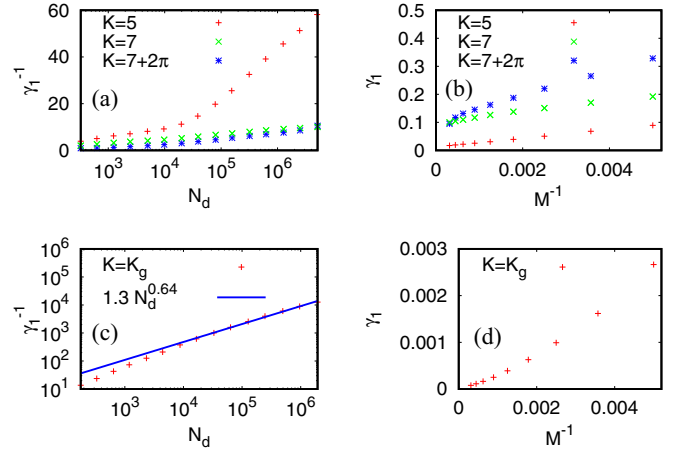

FIG. 9. Dependence of the decay rate $\gamma_1 = -2 \ln |\lambda_1|$ on network size where λ_1 is the second eigenvalue of the UPFO for the Chirikov standard map. Top panels correspond to the values $K = 5, 7, 7 + 2\pi$ [(a) and (b)] and bottom panels [(c) and (d)] to $K = K_g$. Left panels show the dependence of γ_1^{-1} on network size N_d with a logarithmic representation for N_d (and also for γ_1^{-1} for bottom panel with $K = K_g$). Right panels [(b) and (d)] show the dependence of γ_1 on M^{-1} where $N_d \approx M^2/2$ ($M^2/4$) for the cases with $K \geqslant 5$ ($K = K_g$). The blue line in bottom left panel corresponds to the power law fit: $\gamma_1^{-1} = C(N_d)^b$ with $C = 1.3 \pm 0.2$ and $b = 0.64 \pm 0.01$ for the fit range $N_d > 10^4$.

typical localized initial state converges exponentially versus a (roughly) uniform stationary distribution (for the accessible cells) as $\sim \exp(-\gamma_1 t/2)$, where the decay rate is given by $\gamma_1 = -2 \ln(|\lambda_1|)$ in terms of the second eigenvalue λ_1 of the UPFO (with the first eigenvalue always being $\lambda_0 = 1$ for a nondissipative map and its eigenvector being the stationary homogeneous density distribution over the chaotic component in the phase plane).

First results for γ_1 were given for the Chirikov standard map in Ref. [22] and the Arnold cat map in Ref. [34]. Here we present new results for γ_1 obtained by the Arnoldi method for additional values of K and larger M. In most cases an Arnoldi dimension of $n_A = 1000$ (see Ref. [22] for computational details) is largely sufficient to get numerical precise values of γ_1 as well as a considerable amount of largest complex eigenvalues. Only for the Chirikov standard map at $K = K_g$, where the eigenvalue density close to the complex unit circle is rather elevated, did we use $n_A = 3000$ (4000) for $M \leqslant 1600$ ($1600 < M \leqslant 3200$).

Figure 9 shows two different representations of the dependence of γ_1 on M or $N_d \sim M^2$ for the standard map and our usual values $K = K_g, 5, 7, 7 + 2\pi$. For $K \geqslant 5$ the plot of the top left panel seems to indicate that $\gamma_1^{-1} \sim C_1 + C_2 \ln(N_d)$ (with two different regimes for $K = 5$) possibly indicating that $\gamma_1 \sim 1/\ln(N_d) \to 0$ for very large system size. However, the alternative plot of γ_1 versus $1/M$ in top right panel might indicate a finite limit of γ_1 for $M \to \infty$ at least for $K = 7$ with a very particular classical behavior due to the stable island [31] visible in Fig. 4 (bottom left panel). We think that the numerical data does not allow us to conclude clearly if the infinite-size limit of γ_1 is vanishing or finite

since the possible logarithmic behavior may manifest itself at extremely large values of M or N_d numerically not accessible.

For $K = K_g$ we confirm the power law behavior $\gamma_1^{-1} \approx 1.3 \, N_d^{0.64}$ for $N_d > 10^4$ in agreement with the results of Ref. [22]. However, as discussed in Ref. [22], taking into account the data with $N_d < 10^4$ one may also try a more complicated fit using a rational function in $1/M$ providing a different behavior $\gamma_1^{-1} \sim N_d^{0.5} \sim M$ but this would be visible only for extremely large, numerically inaccessible, values of M. Thus for the case $K = K_g$ we can safely conclude that $\gamma_1 \to 0$ for $M \to \infty$ in agreement with the power-law statistics of the Poincaré recurrence time at $K = K_g$.

Concerning the Arnold cat map, the very efficient algorithm to compute the UPFO described in Appendix combined with the Arnoldi method allows us to treat rather large values of M, e.g., up to $M = 983$ corresponding to $N_d \approx 3 \times 10^6$. We remind that due to the necessity to store simultaneously $\sim n_A$ vectors of size N_d it is not possible to consider the Arnoldi method for values such as $M = 14\,699$ for which we were able to compute the Erdös number only using the network link structure. We find that apart from $\lambda_0 = 1$ (nearly) all real and complex eigenvalues of the UPFO are double degenerate due to the symmetry $p \to -p$ and $x \to -x$. Therefore we also implemented a symmetrized version of the UPFO for the cat map where cells at $p_i < 0$ are identified with the corresponding cell at $p_i > 0$ (and $x_i \to -x_i$). This allows the reduction of N_d by roughly a factor of two (cells at $p_i = 0$ are kept as such) and lifts the degeneracy allowing to obtain more *different* eigenvalues at given value of n_A. For small values of M the symmetrized version may miss a few eigenvalues but at $M = 983$ we find that the spectra coincide numerically (for the amount of reliable eigenvalues which we were able to compute for the nonsymmetrized UPFO). Concerning the computation of γ_1 this point is not important since $n_A = 100$ is already sufficient (both symmetrized and nonsymmetrized UPFO) but we verified all γ_1 values also with $n_A = 1000$. However, the symmetrized UPFO allows to obtain larger spectra with less effort.

The left panel of Fig. 10 shows the dependence of γ_1^{-1} on M for $2 \leqslant L \leqslant 5$ and we see for all cases a clear convergence for $M \to \infty$ with final constant values already for $M > 50$. The numerical values of γ_1 can be explained by the diffusive dynamics (3) in p direction with $D = 1/12$ which is expected to be valid for sufficiently large L. Assuming periodic boundary conditions in p direction the diffusive dynamics implies the classical theoretical decay rate $\gamma_1^{(\mathrm{diff})} = D(2\pi)^2/L^2 = \pi^2/(3L^2)$ which agrees quite accurately with our numerical values for $L \geqslant 3$ (this was also seen in Ref. [34] for smaller M values). Only for $L = 2$ the numerical value of γ_1^{-1} is roughly a third larger than the theoretical value which is not astonishing due to the modest value of $L = 2$ limiting the applicability of the diffusive model.

Furthermore, we show as illustration in the right panel of Fig. 10 the top spectrum of $\sim$4000 eigenvalues for the case $M = 983$, $L = 3$ obtained by the Arnoldi method for $n_A = 5000$ applied to the symmetrized UPFO. We note that apart from both top eigenvalues ($\lambda_0 = 1$ and $\lambda_1 \approx 0.834183$) the spectrum is limited to a complex circle of radius ≈ 0.6 with a quite particular pattern for the top eigenvalues with $0.55 < |\lambda_j| < 0.6$ and a cloud of lower eigenvalues with $|\lambda_j| < 0.55$.
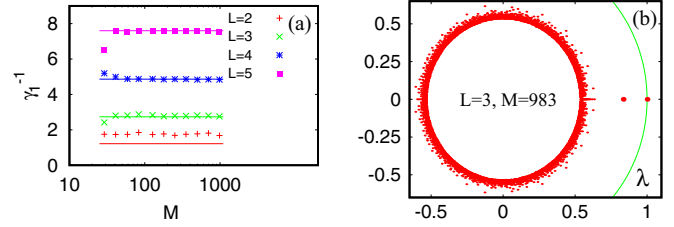

FIG. 10. (a) Dependence of the inverse decay rate $\gamma_1^{-1} = (-2 \ln |\lambda_1|)^{-1}$ on M where λ_1 is the second eigenvalue of the UPFO for the Arnold cat map for the cases $L = 2$, 3, 4, 5 and certain prime numbers $29 \leqslant M \leqslant 983$. The horizontal lines correspond to the theoretical values $[\gamma_1^{(\mathrm{diff})}]^{-1} = [D(2\pi)^2/L^2]^{-1} = 3L^2/\pi^2$ based on diffusive dynamics in the p direction with diffusion constant $D = 1/12$, finite system size L, and periodic boundary conditions. (b) Complex spectrum of top $\sim$4000 reliable eigenvalues λ_j of the UPFO for the Arnold cat map at $L = 3$, $M = 983$ obtained by the Arnoldi method with Arnoldi dimension 5000 and using a symmetrized version of the map in p direction for $0 \leqslant p < L/2$ [symmetrized matrix size $N_d^{(\mathrm{sym})} \approx LM^2/2 \approx 1.5 \times 10^6$]. The green curve corresponds to the unit circle. The first two eigenvalues $\lambda_0 = 1$ and $\lambda_1 \approx 0.834183$, corresponding to $\gamma_1 \approx 0.362604$, are shown as red dots of increased size.

The results of Fig. 10 for the Arnold cat map clearly show that the Erdös number, shown in Fig. 3, is not directly related with the relaxation time $1/\gamma_1$ of the UPFO. As already discussed above on an example of a diffusive process this is related to the fact that the Erdös number does not take into account the variations of transition weights and measures the time when a cell is first touched, leading to a ballistic type of propagation instead of diffusion, while the relaxation time measures the convergence to the stationary homogeneous probability distribution for long time scales.

VI. DISCUSSION

We analyzed the properties of Ulam networks generated by dynamical symplectic maps. Our results show that in the case of strongly chaotic dynamics these networks belong to the class of small-world networks with the number of degrees of separation, or the Erdös number N_E, growing logarithmically with the network size N_d. This growth is related to the Lyapunov exponent of chaotic dynamics. However, the obtained results show that in presence of significant stability islands the Erdös number growth is stronger with $N_E \sim N_d^{0.3}$ being related to orbits sticking in a vicinity of islands. We also show that the Erdös number is not directly related to the largest relaxation times which remain size independent in the case of a diffusive process like for the Arnold cat map on a long torus. We hope that our results will stimulate further useful inter-exchange between the fields of dynamical systems and directed complex networks.

APPENDIX: EXACT UPFO FOR THE ARNOLD CAT MAP

The exact linear form of (2) allows to compute *exactly* (without any averaging procedure) the transition probabilities needed for the UPFO of the Arnold cat map. For this we write each phase-space point in the form $x = x_i \Delta s + \Delta x$ and $p = p_i \Delta s + \Delta p$ with $\Delta s = 1/M$ being the linear cell size and x_i, p_i being integer values. Depending on the parity of M (or LM) we have $0 \leqslant \Delta x < \Delta s$ ($0 \leqslant \Delta p < \Delta s$) for even M (even LM) or $-\Delta s/2 \leqslant \Delta x < \Delta s/2$ ($-\Delta s/2 \leqslant \Delta p < \Delta s/2$) for odd M (odd LM) such that each value of the integer vector (x_i, p_i) corresponds exactly to one Ulam cell. The image of the grid point $\Delta s(x_i, p_i)$ by the cat map is exactly another grid point $\Delta s(\bar{x}_i, \bar{p}_i)$ with integer values $\bar{x}_i$ and $\bar{p}_i$. These grid points are either at the left (bottom) corner/boundary of the corresponding Ulam cell for even values of M (or ML) or in the middle of the Ulam cell for odd values of M (or ML).

The image of an initial Ulam square cell under the Arnold cat map becomes a parallelogram of the same area, spanned by the two vectors $(\Delta s, \Delta s)$ and $(2\Delta s, \Delta s)$, which intersects with 4 (both M and LM even), 5 (both M and LM odd), or 6 target cells (M odd but LM even) as can be seen in Fig. 11. The relative intersection areas of the parallelogram with each cell provide the exact theoretical transition probabilities given as multiples of small powers of $1/2$. For example for the most relevant case of this work, where both M and LM are odd, there are for each initial cell one target cell with transition probability of $1/2$ and four other target cells with probability $1/8$. For the other cases we have four target cells with probability $1/4$ (both M and LM even) or two target cells with probability $3/8$ and four target cells with probability $1/16$ (M odd and LM even).

Furthermore, Fig. 11 also shows the relative positions of the concerned target cell with respect to a reference point being the image of the grid point of the initial Ulam cell. In this way it is possible to compute very efficiently and directly the *exact* Ulam network for the Arnold cat map which allowed us to choose M up to $M = 14\,699$ corresponding to the network size $N_d = LM^2 \approx 6.5 \times 10^8$. We have also verified that our exact computation scheme is in agreement with the two other variants of the Ulam method (apart from statistical fluctuations in the latter).

We may also try a similar analysis of the UPFO for the Chirikov standard map which gives three complications: (i) the standard map is only locally linear for large values of M and the scheme will only be approximate due to nonlinear corrections; (ii) we have to add a certain (rather random/complicated) offset $\xi_0 \Delta s$ [with $\xi_0 = K \sin(2\pi x_i \Delta s)/(2\pi \Delta s) \mod 1$] in the above expressions in terms of x_i or p_i since an initial point on the integer grid is no longer exactly mapped to another point of this grid as it was the case with the Arnold cat map; and, finally, (iii) the parallelogram is now spanned by the two vectors $\Delta s(1, 1)$ and $\Delta s(1 + A, A)$. Here the parameter $A \approx K \cos(2\pi \Delta s \, x_i)$ may take rather large values depending on K and depends on the phase-space position $x \approx \Delta s \, x_i$. The bottom right panel
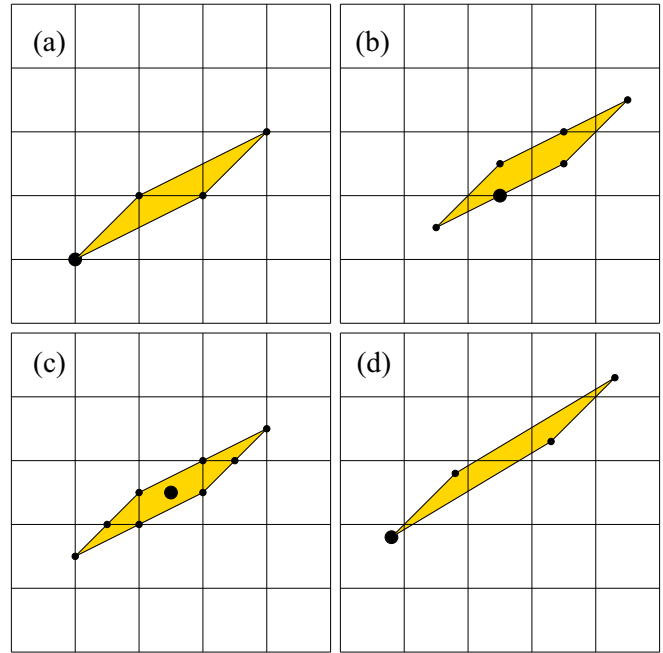

FIG. 11. Parallelogram image of one initial square Ulam cell shown in the grid of possible target cells. The panels correspond to the Arnold cat map with both M and LM even (a), M odd and LM even (b), both M and LM odd (c), and the Chirikov standard map with parameters $\xi_0 = 0.8$ and $A = 1.5$ (d). The thick black dots correspond to the map image of a reference point on the grid $(x_i \Delta s, p_i \Delta s)$ with integer x_i, p_i and linear cell size $\Delta s = 1/M$. The relative intersection areas of the parallelogram with possible target cells provide exactly (approximately) the transition probability of the UPFO for the cat (standard) map. For the Arnold cat map we have four target cells with probability $1/4$ (both M and LM even), two target cells with probability $3/8$ and four target cells with probability $1/16$ (M odd and LM even) or one target cell with probability $1/2$ and four target cells with probability $1/8$ (both M and LM odd).

of Fig. 11 shows an example of such a shifted parallelogram with $\xi_0 = 0.8$ and $A = 1.5$.

For these reasons, this scheme is not suitable to construct numerically a reliable UPFO for the map (1). However, it is still very useful to understand quite well the distribution of the number N_l of connected cells from one initial cell and also the square root singularity in the distribution of weights $p_w(w_l)$ of the UFPO for the standard map (see discussions in Sec. IV for both points).

We note that the obtained UPFO for the Arnold cat map gives us the Markov transition probabilities from one cell to another. The weights of transitions from one cell to others is given by the matrix elements in the corresponding matrix column. The time evolution is obtained by a multiplication of an initial state vector by the matrix. On a physical grounds such evolution corresponds to the exact dynamics given by the Arnold cat map with an additional noise which amplitude is comparable with the cell size. We also note that here we consider the map with a few period cells L in the momentum direction with $L > 1$, while the usually considered case is $L = 1$ (see, e.g., Ref. [3]).

[1] S. M. Ulam, *A Collection of Mathematical Problems*, Vol. 8 of Interscience Tracts in Pure and Applied Mathematics (Interscience, New York, 1960), p. 73.

[2] A. A. Markov, *Rasprostranenie zakona bol'shih chisel na velichiny, zavisyaschie drug ot druga*, Izvestiya Fiziko-matematicheskogo obschestva pri Kazanskom universitete, 2-ya seriya, **15**, 135 (1906) (in Russian) [English trans.: *Extension of the Limit Theorems of Probability Theory to a Sum of Variables Connected in a Chain*, reprinted in Appendix B of: R. A. Howard *Dynamic Probabilistic Systems*, Vol 1: *Markov Models* (Dover, London, 2007)].

[3] A. J. Lichtenberg and M. A. Lieberman, *Regular and Chaotic Dynamics* (Springer, Berlin, 1992).

[4] P. Cvitanovic, R. Artuso, R. Mainieri, G. Tanner, G. Vattay, N. Whelan, and A. Wirsba, *Chaos: Classical and Quantum* (Niels Bohr Institute, Copenhagen, 2016).

[5] T.-Y. Li, Finite approximation for the Perron-Frobenius operator, a solution to Ulam's conjecture, J. Approx. Theory **17**, 177 (1976).

[6] Z. Kovács and T. Tél, Scaling in multifractals: Discretization of an eigenvalue problem, Phys. Rev. A **40**, 4641 (1989).

[7] Z. Kaufmann, H. Lustfeld, and J. Bene, Eigenvalue spectrum of the Frobenius-Perron operator near intermittency, Phys. Rev. E **53**, 1416 (1996).

[8] G. Froyland, R. Murray, and D. Terhesiu, Efficient computation of topological entropy, pressure, conformal measures, and equilibrium states in one dimension, Phys. Rev. E **76**, 036702 (2007).

[9] J. Ding and A. Zhou, Finite approximations of Frobenius-Perron operators: A solution of Ulam's conjecture to multidimensional transformations, Physica D **92**, 61 (1996).

[10] M. Blank, G. Keller, and C. Liverani, Ruelle-Perron-Frobenius spectrum for Anosov maps, Nonlinearity **15**, 1905 (2002).

[11] D. Terhesiu and G. Froyland, Rigorous numerical approximation of Ruelle-Perron-Frobenius operators and topological pressure of expanding maps, Nonlinearity **21**, 1953 (2008).

[12] G. Froyland, S. Lloyd, and A. Quas, Coherent structures and isolated spectrum for Perron–Frobenius cocycles, Ergod. Th. Dynam. Sys. **30**(3), 729 (2010).

[13] C. Schütte, A. Fischer, W. Huisinga, and P. Deuflhard, A direct approach to conformational dynamics based on hybrid Monte Carlo, J. Comput. Phys. **151**, 146 (1999).

[14] G. Froyland and K. Padberg, Almost-invariant sets and invariant manifolds—Connecting probabilistic and geometric descriptions of coherent structures in flows, Physica D **238**, 1507 (2009).

[15] D. L. Shepelyansky and O. V. Zhirov, Google matrix, dynamical attractors and Ulam networks, Phys. Rev. E **81**, 036213 (2010).

[16] L. Ermann and D. L. Shepelyansky, Ulam method and fractal Weyl law for Perron-Frobenius operators, Eur. Phys. J. B **75**, 299 (2010).

[17] S. Brin and L. Page, The anatomy of a large-scale hypertextual Web search engine, Computer Networks and ISDN Systems **30**, 107 (1998).

[18] A. M. Langville and C. D. Meyer, *Google's PageRank and Beyond: The Science of Search Engine Rankings* (Princeton University Press, Princeton, NJ, 2006).

[19] L. Ermann, K. M. Frahm and D. L. Shepelyansky, Google matrix analysis of directed networks, Rev. Mod. Phys. **87**, 1261 (2015).

[20] B. V. Chirikov, A universal instability of many-dimensional oscillator systems, Phys. Rep. **52**, 263 (1979).

[21] V. Arnold and A. Avez, *Ergodic Problems in Classical Mechanics* (Benjamin, New York, 1968).

[22] K. M. Frahm and D. L. Shepelyansky, Ulam method for the Chirikov standard map, Eur. Phys. J. B **76**, 57 (2010).

[23] S. Milgram, The small-world problem, Psychol. Today **1**, 61 (1967).

[24] D. J. Watts and S. H. Strogatz, Collective dynamics of "small-world" networks, Nature **393**, 440 (1998).

[25] M. E. J. Newman, The structure and function of complex networks, SIAM Rev. **45**, 167 (2003).

[26] S. Dorogovtsev, *Lectures on Complex Networks* (Oxford University Press, Oxford, 2010).

[27] L. Backstrom, P. Boldi, M. Rosa, J. Ugander, and S. Vigna, *Four Degrees of Separation*, in Proceeedings of the 4th ACM Web Science Conference (ACM, New York, 2012), p. 33.

[28] B. Chirikov and D. Shepelyansky, Chirikov standard map, Scholarpedia **3**, 3550 (2008).

[29] R. S. MacKay, A renormalisation approach to invariant circles in area-preserving maps, Physica D **7**, 283 (1983).

[30] R. S. MacKay and I. C. Percival, Converse KAM: Theory and practice, Commun. Math. Phys. **98**, 469 (1985).

[31] B. V. Chirikov, Critical perturbation in standard map: A better approximation, arXiv:nlin/0006021[nlin.CD] (2000).

[32] J. D. Meiss, Symplectic maps, variational principles, and transport, Rev. Mod. Phys. **64**, 795 (1992).

[33] B. Georgeot and D. L. Shepelyansky, Quantum computer inverting time arrow for macroscopic systems, Eur. Phys. J. D **19**, 263 (2002).

[34] L. Ermann and D. L. Shepelyansky, The Arnold cat map, the Ulam method and time reversal, Physica D **241**, 514 (2012).

[35] P. Erdös and A. Rényi, On random graphs I, Publ. Math. **6**, 290 (1959).

[36] B. V. Chirikov, Poincaré recurrences in microtron and the global critical structure, arXiv:nlin/0006013[nlin.CD] (2000).

[37] B. V. Chirikov and D. L. Shepelyansky, Asymptotic Statistics of Poincaré Recurrences in Hamiltonian Systems with Divided Phase Space, Phys. Rev. Lett. **82**, 528 (1999).

[38] G. Cristadoro and R. Ketzmerick, Universality of Algebraic Decays in Hamiltonian Systems, Phys. Rev. Lett. **100**, 184101 (2008).

[39] K. M. Frahm and D. L. Shepelyansky, Poincaré recurrences and Ulam method for the Chirikov standard map, Eur. Phys. J. B **86**, 322 (2013).

[40] O. Alus, S. Fishman and J. D. Meiss, Universal exponent for transport in mixed Hamiltonian dynamics, Phys. Rev. E **96**, 032204 (2017).